Sequence Impedance Modeling of Grid-Forming Converters

Preprint

Weihang Yan,[1] Shahil Shah,[1] Vahan Gevorgian,[1] and David Wenzhong Gao[2]

1 National Renewable Energy Laboratory
2 University of Denver

Presented at the 2021 IEEE Power and Energy Society General Meeting
July 25–29, 2021

NREL is a national laboratory of the U.S. Department of Energy
Office of Energy Efficiency & Renewable Energy
Operated by the Alliance for Sustainable Energy, LLC

This report is available at no cost from the National Renewable Energy Laboratory (NREL) at www.nrel.gov/publications.

Contract No. DE-AC36-08GO28308

Conference Paper
NREL/CP-5D00-78234
July 2021

Sequence Impedance Modeling of Grid-Forming Converters

Preprint

Weihang Yan,[1] Shahil Shah,[1] Vahan Gevorgian,[1] and David Wenzhong Gao[2]

1 National Renewable Energy Laboratory
2 University of Denver

Suggested Citation
Yan, Weihang, Shahil Shah, Vahan Gevorgian, and David Wenzhong Gao. 2021. *Sequence Impedance Modeling and Analysis of Grid-Forming Converters: Preprint*. Golden, CO: National Renewable Energy Laboratory. NREL/CP-5D00-78234. https://www.nrel.gov/docs/fy21osti/78234.pdf.

NREL is a national laboratory of the U.S. Department of Energy
Office of Energy Efficiency & Renewable Energy
Operated by the Alliance for Sustainable Energy, LLC

This report is available at no cost from the National Renewable Energy Laboratory (NREL) at www.nrel.gov/publications.

Contract No. DE-AC36-08GO28308

Conference Paper
NREL/CP-5D00-78234
July 2021

National Renewable Energy Laboratory
15013 Denver West Parkway
Golden, CO 80401
303-275-3000 • www.nrel.gov

NOTICE

This work was authored in part by the National Renewable Energy Laboratory, operated by Alliance for Sustainable Energy, LLC, for the U.S. Department of Energy (DOE) under Contract No. DE-AC36-08GO28308. Funding provided by the U.S Department of Energy Office of Energy Efficiency and Renewable Energy Wind Energy Technologies Office. The views expressed herein do not necessarily represent the views of the DOE or the U.S. Government.

Cover Photos by Dennis Schroeder: (clockwise, left to right) NREL 51934, NREL 45897, NREL 42160, NREL 45891, NREL 48097, NREL 46526.

Sequence Impedance Modeling of Grid-Forming Inverters

Weihang Yan[1], Shahil Shah[1], Vahan Gevorgian[1], and David Wenzhong Gao[2]

[1]National Renewable Energy Laboratory (NREL)
Golden, CO 80401, USA
Email: {Weihang.Yan, Shahil.Shah, Vahan.Gevorgian}@nrel.gov

[2]University of Denver
Denver, CO 80208, USA
Email: David.Gao@du.edu

***Abstract*—Grid-forming control of inverter-based resources has been identified as a critical technology for operating power systems with high levels of inverter-based resources. This paper presents the sequence impedance modeling of a grid-forming inverter to evaluate its small-signal stability properties. Droop control structure is implemented to control the inverter in grid-forming mode, and the impact of individual controller on the inverter impedance characteristics is discussed. The developed sequence impedance model is compared with that of the grid-following inverter. It is found from the developed sequence impedance models that grid-forming inverters are less prone to harmonic resonance problems during operation with weaker grids. The developed models are validated using PSCAD simulations.**

***Index Terms*--Impedance modeling, grid-forming inverter, grid-following inverter, stability.**

I. Introduction

Synchronous generators have been responsible for regulating the frequency and magnitude of voltages at different nodes in the bulk power system—they basically "form" the grid by behaving as voltage sources. On the other hand, inverter-based resources (IBRs)—interfacing renewable energy resources and battery energy storage systems—operate in so-called grid-following (GFL) mode by behaving as current sources. They basically "feed" the grid formed by synchronous generators. Even though various grid-supporting functions were proposed for GFL inverters, they maintain the characteristics of current sources and rely on the existence of a strong grid. This prevents the applicability of some possible grid-supporting services, such as black-start capability and rate-of-change-of-frequency support. With the increasing levels of IBRs, however—nearing 100% in some islands and microgrid systems—certain IBRs must be operated as voltage sources, i.e., in grid-forming (GFM) mode to help maintain the stability of the system [1]–[3].

Various control methods have been explored for operating IBRs in GFM mode, including droop control [2], [3], virtual synchronous generator [4]–[6] and virtual oscillator control [7]. Droop control has the simplest implementation, and its reliability has been proven in several microgrid applications [8]. The performance of droop control for implementing GFM functionality in utility scale inverters has also been demonstrated in several industrial projects [9], [10]. Droop-based voltage control of GFM inverters can be implemented either directly using a single-loop architecture or, on top of current control, using a multi-loop architecture [3], [11]. The voltage control in multi-loop architecture that is built on top of fast current control gives greater flexibility in regulating inverter behaviors during transient conditions such as faults; for instance, the inner-loop current control can prevent the inverter from over currents during faults.

Impedance-based methods have proven effective for the stability analysis of modern power systems with high levels of IBRs, such as wind and PV plants, battery energy storage systems, and HVDC transmission systems [12], [13]. Sequence impedance responses have been used to understand the stability characteristics of GFL inverters. GFL inverters are known to suffer from high-frequency stability problems, such as harmonic resonance that do not affect synchronous generators, particularly during operation under weak grid conditions. Controls of GFL inverters have also caused low-frequency sub-synchronous resonance (SSR) [6]. A few papers have studied the impedance characteristics of GFM inverters [4]–[6], but many questions remain unanswered, such as how the GFM impedance characteristics is formulated by individual controller and how they impact the stability properties of a GFM inverter. The existing impedance models established for GFM inverters assume simplified single-loop voltage control architecture [4]–[6], which as discussed above is not preferred in practical inverters. Also, the reported impedance modeling works for GFM inverters focus more on virtual synchronous generator control instead of droop control, where droop control is more likely to be accepted by the industry for the wide-spread deployment of GFM inverters in bulk power system applications [8]–[10].

This paper presents sequence impedance modeling of GFM inverters using a droop-based multi-loop control architecture. The paper compares the developed GFM impedance model with that of a GFL inverter; it shows that grid-synchronization in GFM inverters using droop control instead of a phase-locked loop (PLL) used in GFL inverters makes GFM inverters less likely to experience harmonic stability problems during operation with weaker grids. The developed sequence impedance models are

This work was authored by Alliance for Sustainable Energy, LLC, the manager and operator of the National Renewable Energy Laboratory for the U.S. Department of Energy (DOE) under Contract No. DE-AC36-08GO28308. Funding provided by U.S. Department of Energy Office of Energy Efficiency and Renewable Energy Wind Energy Technologies Office. The views expressed in the article do not necessarily represent the views of the DOE or the U.S. Government. The U.S. Government retains and the publisher, by accepting the article for publication, acknowledges that the U.S. Government retains a nonexclusive, paid-up, irrevocable, worldwide license to publish or reproduce the published form of this work, or allow others to do so, for U.S. Government purposes.

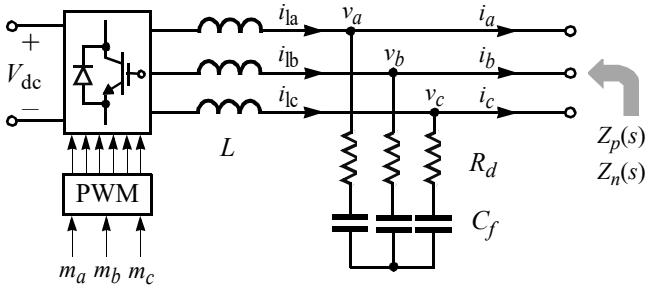

Fig. 1. Circuit diagram of grid-connected voltage source converter.

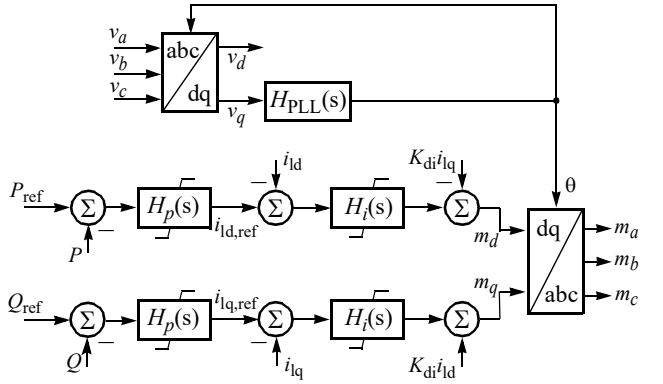

Fig. 2. Control diagram of PI power-controlled GFL inverter.

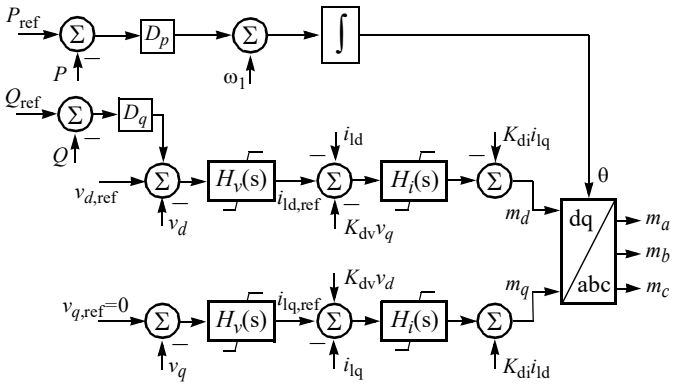

Fig. 3. Control diagram of droop-controlled GFM inverter.

validated by PSCAD simulations of 1 MVA/0.69 kV inverter.

II. Sequence Impedance Modeling

Fig. 1 shows the three-phase grid-connected voltage source converter (VSC) studied in this paper. Three-phase voltages and currents are denoted as v_{abc}, i_{labc} and i_{abc}, respectively, where l indicate currents flow in the filter inductor. Assuming relatively large DC-link capacitors, the DC bus voltage V_{dc} is considered as constant in this paper. The fundamental frequency, f_1, equals 60Hz; and the nominal angular speed is $\omega_1=2\pi f_1$. Modulation signals for power switches are represented as m_{abc} within the inverter average model [12]. The inductance, capacitance, and damping resistance of the LC filter are denoted as L, C_f, and R_d, respectively. $Z_p(s)$ and $Z_n(s)$ denote the positive and negative sequence impedances of the VSC.

Fig. 2 and Fig. 3 show the controls of the VSC under GFL and GFM operation modes, where P_{ref} and Q_{ref} are the power references. The instantaneous active and reactive power outputs to the grid, P and Q, are written in terms of the dq-axis components of the voltages and currents at the point of common coupling (PCC), as in (1) and (2):

$$P = \frac{3}{2} G_p(s)(v_d i_d + v_q i_q) \tag{1}$$

$$Q = \frac{3}{2} G_p(s)(v_q i_d - v_d i_q) \tag{2}$$

where G_p(s) represents the low-pass filter for power smoothing.

As shown in Fig. 2, in GFL operation mode, the outer-loop PI compensators, H_p(s), control the active and reactive power, and they further generate current references, $i_{ld,ref}$ and $i_{lq,ref}$, for the inner-loop current controllers, $H_i(s)$. A PLL is used to obtain the grid voltage angle, θ, required for synchronization. On the other hand, for GFM operation mode, as shown in Fig. 3, voltage controllers $H_v(s)$ are implemented on top of the current controls instead of power controls as done for GFL operation mode. The current references, $i_{ld,ref}$ and $i_{lq,ref}$, are generated to regulate inverter output currents, and they provide current-limiting function. Decoupling terms are $K_{di}=\omega_1 L$ and $K_{dv}=\omega_1 C_f$. The reference for the q-axis component of the voltage, $v_{q,ref}$, is set to zero for simplicity; hence, the voltage reference on the d-axis, $v_{d,ref}$, represents the magnitude reference of the PCC voltages. The frequency of voltages is controlled by droop characteristics, and it further adds a nominal angular frequency to derive phase θ. Active power-frequency and reactive power-voltage droop controls are implemented as active and reactive power loops, with droop coefficients of D_p and D_q, respectively.

Under a small-signal perturbation at positive-sequence frequency f_p, the phase a voltage of the VSC output in the time domain can be written as in (3):

$$v_a(t) = V_1 \cos(2\pi f_1 t) + V_p \cos(2\pi f_p t + \phi_{vp}) \tag{3}$$

where V_1 is the amplitude of the voltage at the fundamental frequency, f_1. V_p and ϕ_{vp} correspond to the amplitude and phase angle of the positive-sequence perturbation. Voltages of phase b and c under perturbation can be derived similarly.

Phase a voltage in the frequency domain is given in (4):

$$\mathbf{V}_a[f] = \begin{cases} \frac{1}{2} V_1 & f = f_1 \\ \frac{1}{2} V_p e^{\pm j\phi_{vp}} & f = \pm f_p \end{cases} \tag{4}$$

here, the positive-sequence perturbation component $\mathbf{V}_p=\mathbf{V}_a[\pm f_p]$. Under the perturbation, three-phase currents can be similarly described. Then, referring to [12] and [13], the positive-sequence impedance of the VSC, $Z_p(s)$, is defined as the ratio of $\mathbf{V}_p$ to $-\mathbf{I}_p$.

Because of the perturbation on the PCC voltages, the synchronous frame is displaced from the rotating frame of the grid voltage by angle of $\Delta\theta(t)$. Note that the derivations of $\Delta\theta(t)$ for GFL and GFM inverters are different. As illustrated in Fig. 2 and Fig. 3, GFL inverters use a PLL to achieve grid synchronization. On the other hand, GFM inverters use active power flow equation, similar to that of synchronous machines, to control phase angle

displacement. In general, assuming $\theta_1(t)=\omega_1 t$, the phase output of VSC, $\theta(t)$, can be written as in (5):

$$\theta(t) = \theta_1(t) + \Delta\theta(t) \tag{5}$$

Therefore, by implementing Park's transformation, the three-phase voltages of the VSC in the frequency domain are expressed as in (6) and (7):

$$\mathbf{V}_d[f] = \begin{cases} V_1 & f = 0 \\ \mathbf{V}_p & f = \pm(f_p - f_1) \end{cases} \tag{6}$$

$$\mathbf{V}_q[f] = \begin{cases} 0 & f = 0 \\ \mp j\mathbf{V}_p - V_1\Delta\boldsymbol{\theta}[f] & f = \pm(f_p - f_1) \end{cases} \tag{7}$$

Similarly, currents in the inductors, $\mathbf{I}_{\mathrm{ld}}$ and $\mathbf{I}_{\mathrm{lq}}$, can be presented as in (8) and (9):

$$\mathbf{I}_{\mathrm{ld}}[f] = \begin{cases} I_{l1}\cos\varphi_{l1} & f = 0 \\ \mathbf{I}_{\mathrm{lp}} + I_{l1}\sin\varphi_{l1}\Delta\boldsymbol{\theta}[f] & f = \pm(f_p - f_1) \end{cases} \tag{8}$$

$$\mathbf{I}_{\mathrm{lq}}[f] = \begin{cases} I_{l1}\sin\varphi_{l1} & f = 0 \\ \mp j\mathbf{I}_{\mathrm{lp}} - I_{l1}\cos\varphi_{l1}\Delta\boldsymbol{\theta}[f] & f = \pm(f_p - f_1) \end{cases} \tag{9}$$

Further, denoting Laplace operator $s=j2\pi f_p$, the output currents at the PCC, $\mathbf{I}_d$ and $\mathbf{I}_q$, are derived as in (10) and (11), considering the filter impedance, $Z_f(s)$.

$$\mathbf{I}_d[f] = \begin{cases} I_1\cos\varphi_1 & f = 0 \\ \mathbf{I}_{\mathrm{lp}} - \dfrac{\mathbf{V}_p}{Z_f(s)} + I_1\sin\varphi_1\Delta\boldsymbol{\theta}[f] & f = \pm(f_p - f_1) \end{cases} \tag{10}$$

$$\mathbf{I}_q[f] = \begin{cases} I_1\sin\varphi_1 & f = 0 \\ \mp j\mathbf{I}_{\mathrm{lp}} \pm \dfrac{j\mathbf{V}_p}{Z_f(s)} - I_1\cos\varphi_1\Delta\boldsymbol{\theta}[f] & f = \pm(f_p - f_1) \end{cases} \tag{11}$$

Summarizing (6)–(11), V_1, $\mathbf{I}_{l1}=I_{l1}\cos\varphi_{l1}+jI_{l1}\sin\varphi_{l1}$, and $\mathbf{I}_1=I_1\cos\varphi_1+jI_1\sin\varphi_1$ are steady-state PCC voltages, inductor currents, and PCC output currents, respectively. Impedance $Z_f(s)$, which associates with the capacitance branch of the LC filter, is written as in (12):

$$Z_f(s) = R_d + \frac{1}{sC_f} \tag{12}$$

A. Impedance Modeling of GFL inverter

The sequence impedance model of current-controlled GFL inverters in (13) is the cornerstone of establishing impedance models for power-controlled GFL inverters and droop-controlled GFM inverters [12], [13]. Specifically in (13), k_m is the modulator gain. $\mathbf{M}_1$ is the steady state value of modulating signal m_d+jm_q.

$$Z_p(s) = \frac{sL + k_m V_{\mathrm{dc}}[H_i(s-j\omega_1) - jK_{\mathrm{di}}]}{1 - \dfrac{1}{2}k_m V_{\mathrm{dc}}\{\mathbf{I}_{l1}[H_i(s-j\omega_1) - jK_{\mathrm{di}}] + \mathbf{M}_1\}\dfrac{T_{\mathrm{PLL}}(s-j\omega_1)}{V_1}} \| Z_f(s) \tag{13}$$

Further, $T_{\mathrm{PLL}}(s)$ is denoted as the closed-loop gain of the PLL, which is expressed in (14):

$$T_{\mathrm{PLL}}(s) = \frac{V_1 H_{\mathrm{PLL}}(s)}{1 + V_1 H_{\mathrm{PLL}}(s)} \tag{14}$$

To extend (13) to power-controlled GFL inverters, the power equations in (1) and (2) are linearized as in (15) and (16):

$$P(s) = 1.5G_p(s)[I_1\cos\varphi_1 V_d(s) + V_1 I_d(s) + I_1\sin\varphi_1 V_q(s)] \tag{15}$$

$$Q(s) = 1.5G_p(s)[I_1\cos\varphi_1 V_q(s) - I_1\sin\varphi_1 V_d(s) - V_1 I_q(s)] \tag{16}$$

The current references, $i_{\mathrm{ld,ref}}$ and $i_{\mathrm{lq,ref}}$, of a GFL inverter can be further derived as in (17) and (18), respectively, under small-signal perturbation.

$$I_{\mathrm{ld,ref}}(s) = -H_p(s)P(s) \tag{17}$$

$$I_{\mathrm{lq,ref}}(s) = -H_p(s)Q(s) \tag{18}$$

Combining (10)–(18), the positive-sequence impedance model of a power-controlled GFL inverter can be easily derived by adding term $1.5k_m V_{\mathrm{dc}} V_1 G_p(s-j\omega_1)H_p(s-j\omega_1)H_i(s-j\omega_1)$ on the numerator of (13).

B. Impedance Modeling of GFM inverter

In this section, the impedance model of a droop-controlled GFM inverter is established, where its inner-loop current control is identical to that of a GFL inverter. Similar to a GFL inverter, modulating signals of the VSC under small-signal perturbation are written as in (19) and (20):

$$M_d(s) = H_i(s)[I_{\mathrm{ld,ref}}(s) - I_{\mathrm{ld}}(s)] - K_{\mathrm{di}}I_{\mathrm{lq}}(s) \tag{19}$$

$$M_q(s) = H_i(s)[I_{\mathrm{lq,ref}}(s) - I_{\mathrm{lq}}(s)] + K_{\mathrm{di}}I_{\mathrm{ld}}(s) \tag{20}$$

Different from a power-controlled GFL inverter, GFM directly controls the voltage amplitudes and phase angle of the VSC to

$$Z_p(s) = \frac{sL + k_m V_{\mathrm{dc}}[H_i(s-j\omega_1) - jK_{\mathrm{di}}] + \dfrac{1}{2}k_m V_{\mathrm{dc}} V_1[K_p(s-j\omega_1) - K_q(s-j\omega_1)]}{1 + k_m V_{\mathrm{dc}}[H_v(s-j\omega_1) - jK_{\mathrm{dv}}]H_i(s-j\omega_1) + \dfrac{1}{2}k_m V_{\mathrm{dc}}\left\{\left[\mathbf{I}_1^* - \dfrac{V_1}{Z_f(s)}\right]K_p(s-j\omega_1) + \left[\mathbf{I}_1^* + \dfrac{V_1}{Z_f(s)}\right]K_q(s-j\omega_1)\right\}} \| Z_f(s) \tag{24}$$

where:

$$K_p(s) = j\frac{3}{2}\{V_1[H_v(s) - jK_{\mathrm{dv}}]H_i(s) + \mathbf{I}_{l1}[H_i(s) - jK_{\mathrm{di}}] + \mathbf{M}_1\}G_p(s)\frac{1}{s}D_p\omega_1$$

$$K_q(s) = j\frac{3}{2}D_q V_1 G_p(s)H_v(s)H_i(s)$$

provide grid-supporting functions; hence, the current references of a GFM inverter are derived through outer-loop voltage controllers, $H_v(s)$, which are given in (21) and (22):

$$I_{\mathrm{ld,ref}}(s) = H_v(s)[-D_q Q(s) - V_d(s)] - K_{\mathrm{dv}} V_q(s) \quad (21)$$

$$I_{\mathrm{lq,ref}}(s) = -H_v(s) V_q(s) + K_{\mathrm{dv}} V_d(s) \quad (22)$$

Integrating reactive power-voltage droop D_q in (21) to adjust the voltage amplitude reference, the derivation of the reactive power loop of the droop-controlled GFM inverter is completed.

In this paper, the active power-frequency droop is used for the active power control of the GFM inverter as well as for synchronizing the GFM inverter to the grid; therefore, the phase angle of the VSC under small-signal perturbation, $\Delta\theta(s)$, can be expressed as in (23):

$$\Delta\theta(s) = -\frac{1}{s} D_p \omega_1 P(s) \quad (23)$$

where, the initial frequency deviation is simplified as 0.

Equation (23) completes the derivation of the active power loop of a GFM inverter. Substituting (6)–(12), (15)–(16), and (21)–(23) into (19) and (20), the impedance model of a droop-controlled GFM inverter is derived as in (24). The polynomials $K_p(s)$ and $K_q(s)$ are associated with the grid synchronization dynamics and voltage regulation that are introduced through the droop characteristics.

To derive the negative-sequence impedance model for both the GFL and GFM inverters, (25) can be simply used:

$$Z_n(s) = Z_p(-s)^* \quad (25)$$

III. Impedance Response of GFM Inverters

To establish valid utility scale models for GFM and GFL inverters, many practical VSC design principles are considered; therefore, the VSC inner-loop current control bandwidth is selected as 190 Hz, and the corresponding outer-loop control bandwidth is 10 times slower. The PLL bandwidth is 30 Hz. Note that the voltage control bandwidth of a GFM inverter inevitably depends on the load and line impedances; hence, the rated load condition of a GFM inverter is considered for selecting the parameters of the voltage compensators. Fig. 4 gives the comparative power responses of the modeled GFL and GFM inverters. Detailed modeling and simulation parameters are listed in Table I and Table II.

Fig. 5 presents the comparative impedance responses of the studied GFL and GFM inverters. Apparently, the impedance responses of the GFL and GFM inverters share the same trend in the medium frequency range and converge at a high frequency range, because of the identical inner-loop current control and LC filter. The integration of the outer-loop controller in the GFL inverter mainly increases the amplitude of its impedance response, such that the GFL inverter behaves more like an equivalent current source around the fundamental frequency. The outer-loop controller in the GFM inverter, on the contrary, primarily modifies the denominator of its impedance characteristics by replacing the

TABLE I Inverter Parameters

Parameter	Value
Inverter rated power	1MVA
PCC voltage (peak), V_1	0.563kV
PCC current (peak), I_{o1}	1.082kA
Inductor current (peak), I_{l1}	1.084kA
Filter, L, C_f, R_d	3mH, 22uF, 1.87Ω
DC bus voltage, V_{dc}	2kV

TABLE II Parameters of Inverter Controllers

GFL	GFM
Current compensator, $H_i(s)$= 0.00255 +1/(0.327s)	
Power smoothing filter, $G_p(s)$= 1/(0.02s+1)	
Power compensator $H_p(s)$= 0.0029+1/(8.823s)	Droop coefficients D_p=0.05p.u.; D_q=0.05p.u.
PLL compensator $H_{\mathrm{PLL}}(s)$= [0.237+1/(0.0224s)]/s	Voltage compensator $H_v(s)$= 1.522+1/(0.0047s)

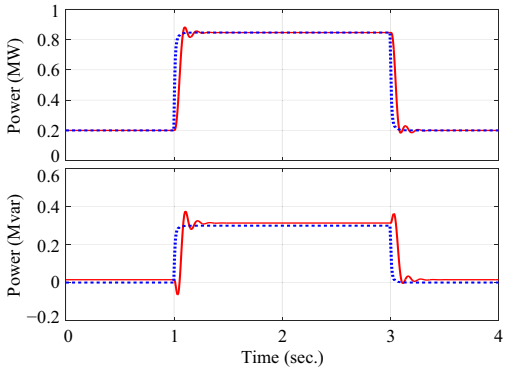

Fig. 4. Power step change responses of GFL and GFM inverters. Blue dashed lines: GFL inverter, red solid lines: GFM inverter.

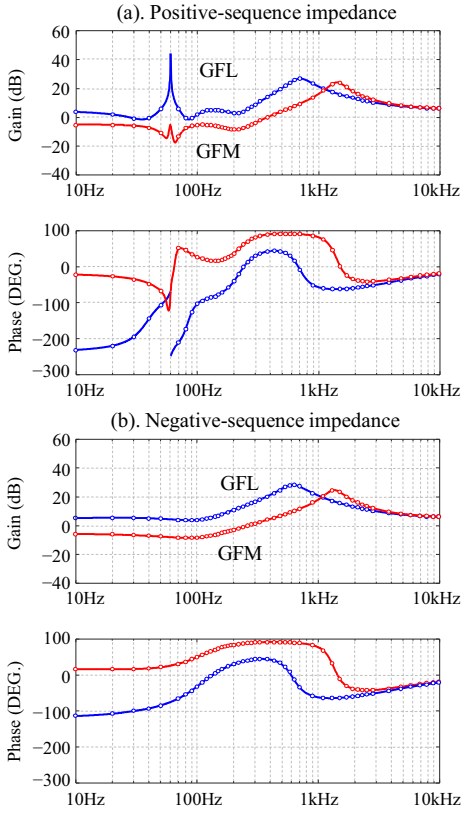

Fig. 5. Impedance response and validation. Blue lines: power-controlled GFL inverter, red lines: droop-controlled GFM inverter, and dots: PSCAD simulation validations.

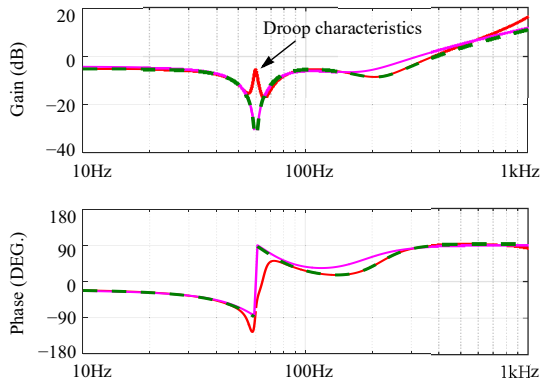

Fig. 6. Simplified impedance models of GFM inverter. Red solid line: detailed GFM model in (24), green dashed line: GFM model in (26), pink solid line: GFM model in (27).

PLL, which further approximates the GFM inverter to an equivalent voltage source. In fact, the droop coefficients of a GFM inverter cannot be large considering the "rotor-angle" stability criterion [14]; hence, they only modify the impedance response of a GFM inverter around its fundamental frequency. By ignoring the droop coefficients and filter capacitance branch, the simplified impedance model can be expressed as in (26).

$$Z_p(s) = \frac{sL + k_m V_{\mathrm{dc}}[H_i(s-j\omega_1) - jK_{\mathrm{di}}]}{1 + k_m V_{\mathrm{dc}}[H_v(s-j\omega_1) - jK_{\mathrm{dv}}]H_i(s-j\omega_1)} \quad (26)$$

Fig. 6 compares the impedance responses of the detailed and the simplified GFM models. It is well studied for GFL inverters that the fast response of the PLL [12], [13] introduces a negative resistance to its impedance response, which increases high-frequency system instability concerns; however, benefiting from the replacement of PLL, a GFM inverter can mitigate such issues and avoid high-frequency instability when connected to a weak grid. Further, because of the different control bandwidths selected for the outer-loop and inner-loop controllers, (26) can be approximately reduced into (27):

$$Z_p(s) = \frac{1}{H_v(s-j\omega_1)} + \frac{sL}{1 + k_m V_{\mathrm{dc}} k_{\mathrm{pv}} H_i(s-j\omega_1)} \quad (27)$$

where k_{pv} is the proportional gain in PI compensator $H_v(s)$. Equation (27) further divides the impedance model of a GFM inverter into two components, such that its first term (voltage controller) dominates the system low-frequency range response and the second term (current controller and filter inductor) dominates the medium-frequency range response.

IV. Conclusions

This paper presents sequence impedance modeling and validation of GFM inverters using a droop-based multi-loop control architecture. The established impedance model reveals the fundamental differences between GFL and GFM inverters. The impact of droop, voltage, and current controllers on the impedance characteristics of GFM inverters is discussed. It shows that grid-synchronization in GFM inverters using droop control instead of a PLL used in GFL inverters makes GFM inverters less likely to experience harmonic stability problems. Different from the existing GFM impedance models, droop-based multi-loop control structure modifies the low frequency range behavior of a GFM impedance model. As a result, a GFM inverter generally presents resistive and capacitive behaviors below the fundamental frequency, which can also prevent the possible SSR when a GFM inverter is connected to a series-compensated network.

References

[1] B. Kroposki, B. Johnson, Y. Zhang, V. Gevorgian, P. Denholm, B. Hodge, and B. Hannegan, "Achieving a 100% renewable grid: operating electric power systems with extremely high levels of variable renewable energy," *IEEE Power and Energy Mag.*, vol. 15, no. 2, pp. 61-73, March-April 2017.

[2] J. Rocabert, A. Luna, F. Blaabjerg, and P. Rodríguez, "Control of power converters in AC microgrids," *IEEE Trans. on Power Electron.*, vol. 27, no. 11, pp. 4734-4749, Nov. 2012.

[3] W. Du, Z. Chen, K. P. Schneider, R. H. Lasseter, S. P. Nandanoori, F. K. Tuffner, and S. Kundu, "A comparative study of two widely used grid-forming droop controls on microgrid small-signal stability," *IEEE Jour. of Emer. and Selected Topics in Power Electron.*, vol. 8, no. 2, pp. 963-975, June 2020.

[4] W. Wu, Y. Chen, L. Zhou, A. Luo, X. Zhou, Z. He, L. Yang, Z. Xie, J. Liu, and M. Zhang, "Sequence impedance modeling and stability comparative analysis of voltage-controlled VSGs and current-controlled VSGs," *IEEE Trans. on Indust. Electron.*, vol. 66, no. 8, pp. 6460-6472, Aug. 2019.

[5] L. Zhou, Z. Shuai, Y. Chen, W. Wu, X. Zhou, K. Yan, and A. Luo, "Impedance-based harmonic current suppression method for VSG connected to distorted grid," *IEEE Trans. on Indust. Electron.*, vol. 67, no. 7, pp. 5490-5502, July 2020.

[6] G. Li, Y. Chen, A. Luo, Z. He, H. Wang, Z. Zhu, W. Wu, and L. Zhou, "Analysis and mitigation of subsynchronous resonance in series-compensated grid-connected system controlled by a virtual synchronous generator," *IEEE Trans. on Power Electron.*, vol. 35, no. 10, pp. 11096-11107, Oct. 2020.

[7] B. B. Johnson, S. V. Dhople, J. L. Cale, A. O. Hamadeh, and P. T. Krein, "Oscillator-based inverter control for islanded three-phase microgrids," *IEEE Jour. of Photovol.*, vol. 4, no. 1, pp. 387-395, Jan. 2014.

[8] R. Panora, J. E. Gehret, M. M. Furse, and R. H. Lasseter, "Real-world performance of a CERTS microgrid in Manhattan," *IEEE Trans. on Sustain. Energy*, vol. 5, no. 4, pp. 1356-1360, Oct. 2014.

[9] O. Schomann, "Experiences with large grid-forming inverters on various island and microgrid projects," in Proc. Hybrid Power Systems Workshop, May 2019, Crete, Greece. [Online]. Available: https://www.sma.de/en/products/references/st-eustatius-caribbean.html

[10] Large-scale battery storage knowledge sharing report, prepared by Aurecon for Australian Renewable Energy Agency (ARENA), Sep. 2019. [Online]. Available: https://arena.gov.au/assets/2019/11/large-scale-battery-storage-knowledge-sharing-report.pdf.

[11] W. Yan, L. Cheng, S. Yan, W. Gao, and D. W. Gao, "Enabling and evaluation of inertial control for PMSG-WTG using Synchronverter with multiple virtual rotating masses in microgrid," *IEEE Trans. on Sustain. Energy*, vol. 11, no. 2, pp. 1078-1088, Apr. 2020.

[12] M. Cespedes and J. Sun, "Impedance modeling and analysis of grid-connected voltage-source converters," *IEEE Trans. on Power Electron.*, vol. 29, no. 3, pp. 1254-1261, March 2014.

[13] S. Shah and L. Parsa, "Impedance modeling of three-phase voltage source converters in dq, sequence, and phasor domains," *IEEE Trans on Energy Conv.*, vol. 32, no. 3, pp. 1139-1150, Sept. 2017.

[14] N. Pogaku, M. Prodanovic, and T. C. Green, "Modeling, analysis and testing of autonomous operation of an inverter-based microgrid," *IEEE Trans. on Power Electron.*, vol. 22, no. 2, pp. 613-625, Mar. 2007.